Eur. Phys. J. D **18**, 69–75 (2002)
DOI: 10.1140/e10053-002-0008-5

THE EUROPEAN PHYSICAL JOURNAL D
EDP Sciences

Photophysics of C_{60} and C_{60}^- in faujasite zeolites

O.-H. Kwon, H. Yoo, and D.-J. Jang[a]

School of Chemistry, Seoul National University, Seoul 151-742, Korea

Received 13 July 2001 and Received in final form 8 October 2001

Abstract. While the intercalation of C_{60} and the formation of C_{60}^- in the supercages of NaX and NaY are confirmed by using ^{129}Xe NMR and ESR, the photophysical properties of C_{60} and C_{60}^- are characterized by monitoring transient reflectance spectra and kinetics, fluorescence kinetics, and diffuse reflectance spectra. C_{60}^- is considerably more abundant in NaY than in NaX. This difference is explained in terms of polarity difference between two zeolites. Both C_{60} and C_{60}^- have remarkably elongated excited-state lifetimes due to their collision-free environment in zeolitic nanocavities although C_{60}^- has much shorter lifetimes than C_{60}. C_{60}^-, in particular, shows intense absorption and emission due to its reduced symmetry in zeolites.

PACS. 33.50.-j Fluorescence and phosphorescence; radiationless transitions, quenching (intersystem crossing, internal conversion) – 78.40.-q Absorption and reflection spectra: visible and ultraviolet – 61.48.+c Fullerenes and fullerene-related materials

1 Introduction

Zeolites have been extensively investigated as they play indispensable roles in many technological and economical applications [1–3]. Their ordered cages and channels are potential hosts to organic and inorganic complexes, and act as reactors in the synthesis of nanoclusters and nanowires [4–6]. Furthermore, optical properties of molecular clusters confined in zeolites have been widely investigated because their electronic properties can be altered by varying the dielectric and charge properties of the nanoporous hosts [7]. Thus they may open up new nanotechnological applications for the heterogeneous catalysts and advanced electronic, magnetic and optical devices.

There have been a great deal of research interests on the physical and chemical properties of C_{60} [8–10] and on the intercalation of C_{60} molecules in the cages and channels of zeolites [11–16]. The incorporation of C_{60} molecules into the robust nanocavities of faujasite zeolites [12–15] would be more interesting than the insertion into the extra large zeolitic pores because there are no physical barriers to immobilize C_{60} into the latter pores. Direct evidences such as ^{129}Xe NMR spectra need to be shown for the intercalation of C_{60} into faujasite zeolitic pores. ^{129}Xe NMR spectroscopy has been used as a sensitive tool to confirm the encapsulation of organic molecules into the faujasite zeolites [17,18].

Although the $^1t_{1g} \leftarrow {}^1h_u$ transition of C_{60} is allowed to reveal strong absorption in 200−400 nm, the $^1t_{1u} \leftarrow {}^1h_u$ transition of C_{60} is first-order forbidden, showing very weak broad absorption in the region of 400−700 nm [19]. The weak fluorescence of $^1t_{1u} \rightarrow {}^1h_u$ transition with the maximum in 650–800 nm has been studied in a variety of systems [20–22]. Transient absorption around 975 and 740 nm is attributed to the excited singlet and lowest triplet states of C_{60}, respectively [23–25]. While the relaxation from the upper-excited singlet state occurs within a few picoseconds [26], the lowest-excited singlet and triplet states of C_{60} in solvents decay on the time scales of 650–1 200 ps and 10–50 μs, respectively, as shown in Figure 1 [24,25].

As C_{60} molecules form charge-transfer complexes with electron donors, the symmetry-forbidden absorption of $t_{1u} \leftarrow h_u$ is reported to increase [27,28]. A strong absorption of C_{60}^- at 1 069 nm has been attributed to the allowed electric-dipolar transition of $^2t_{1g} \leftarrow {}^2t_{1u}$ [29,30]. The formation of the anions is known to give birth to absorption at 350–520 nm as well [27,28]. The dynamics and spectrum of the anionic fluorescence arising from the transition of $^2t_{1u} \rightarrow {}^2h_u$ are hardly studied yet although the fluorescence resulting from $^2t_{1g} \rightarrow {}^2t_{1u}$ transition is reported to have the maximum intensity at 1 140 nm [31]. ESR spectroscopy has been employed to investigate the formation of C_{60}^- in various circumstances [10].

There have been several brief reports on the formation of C_{60} anions in faujasite zeolites [12–14]. However, little has been described about the nature of anions in faujasite zeolites. We report here our close investigation on the formation of C_{60}^- and the photophysics of C_{60}^- and C_{60} in the zeolitic surface of NaX and NaY nanocavities.

2 Experimental

2.1 Materials

C_{60}, purchased from Sigma, was used without further purification. Na^+-exchanged X (NaX) and Y zeolites (NaY)

[a] e-mail: djjang@plaza.snu.ac.kr

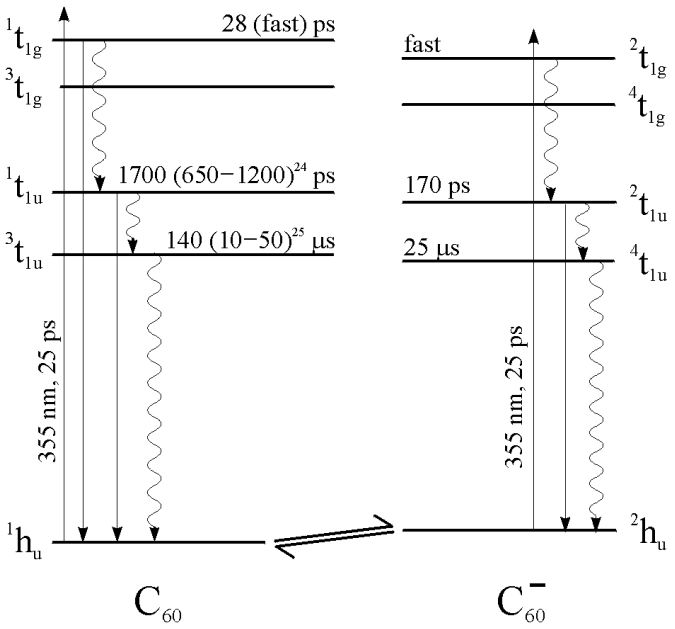

Fig. 1. Schematic representation of the photophysical dynamics of C_{60} and C_{60}^- intercalated in the supercages of faujasite zeolites in a vacuum. The times in parentheses are the lifetimes of solutions reported in the superscripted refs.

of high purity were synthesized, washed with doubly distilled hot water, and dried in a vacuum oven. After dehydration at 400 °C for 5 h and cooling to room temperature, NaX or NaY with 1.0 mmol of the supercage was mixed with 25 μmol of C_{60} in a quartz tube. The tube was evacuated, sealed, maintained at 650 °C for 72 h in order to make C_{60} sublime and diffuse uniformly into zeolite supercages, and then cooled slowly to room temperature. X-ray diffraction was used to confirm that the structures of C_{60}-introduced NaX (C_{60}X) and C_{60}-introduced NaY (C_{60}Y) did not change during the preparation.

2.2 Measurements

^{129}Xe gas (Matheson, 99.995%) was equilibrated with a sample contained in an NMR tube through a stopcock before a ^{129}Xe NMR spectrum was measured using an NMR spectrometer (Bruker, AM-300). ESR derivative curves were measured at X band using an ESR spectrometer (Bruker, ESP 300) with the frequency of 9.7 GHz. The diffuse reflectance spectra were measured using an absorption spectrometer equipped with an integrating sphere (Shimadzu, UV-3101 PC).

The third (355 nm) harmonic pulses having the duration of 25 ps from an actively and passively mode-locked Nd:YAG laser (Quantel, YG 701) were employed to excite samples. Emission kinetics after wavelength selection using combined band-pass filters was detected by using a CCD-attached streak camera having the temporal resolution of 10 ps (Hamamatsu, C2830). Fluorescence kinetic constants were extracted by fitting a measured kinetic profile to a computer-simulated kinetic curve convoluted with the temporal response function iteratively.

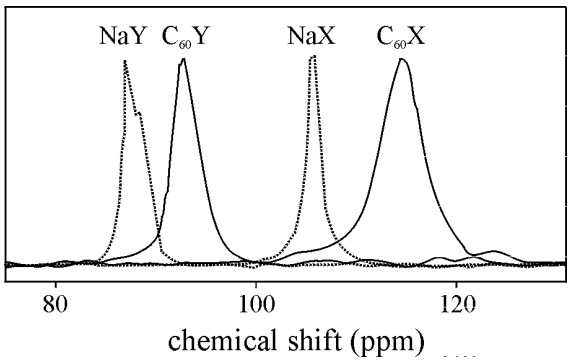

Fig. 2. ^{129}Xe NMR spectra of NaY, C_{60}Y, NaX, and C_{60}X showing the chemical shifts of 87, 93, 105, and 115 ppm, respectively.

A sample was excited by using the pulsed beam of 337 nm having the duration of 0.6 ns from a nitrogen laser (Photonics, LN 1000). The wavelength of the probe beam from a Xe lamp (Schoeffel, LPS 255) was selected by using two monochromators having the path length of 0.275 m (Acton Research, Spectrapro 275). The intensity change of the probe beam reflected from the sample was detected by using a photomultiplier tube (Hamamatsu, R928) which was connected to an oscilloscope of 200 MHz (Tektronix, TDS 350). The laser and the oscilloscope were triggered with variable delays by a pulse/delay generator (Stanford Research Systems, DG 535). All the spectra and kinetic profiles reported here were measured at room temperature.

3 Results

3.1 Intercalation of C_{60} into the supercage of faujasite zeolites

The chemical shift of C_{60}X is larger by 10 ppm than that of NaX while the chemical shift of C_{60}Y is larger by 6 ppm than that of NaY (Fig. 2). The larger chemical shifts of C_{60}-introduced zeolites are due to the strong interactions of Xe atoms with organic C_{60} molecules in addition to collisions with the supercage wall and other xenon atoms present in bare zeolites [18,32]. The observation of a single peak at a new position for each C_{60}-introduced zeolite indicates that the supercages of both zeolites are impregnate with C_{60} molecules uniformly from a macroscopic viewpoint. Considering that only the 0.025 fraction of the supercages contain C_{60} molecules, we think that the chemical shifts are quite large in both zeolites. NaX and C_{60}X reveal larger chemical shifts than NaY and C_{60}Y as reported [17].

Many attempts have been made at various temperatures to intercalate C_{60} into the supercage with keeping the structural integrity, until the optimum temperature is determined to be ∼650 °C for both zeolites. This is about the lowest temperature where C_{60} molecules can

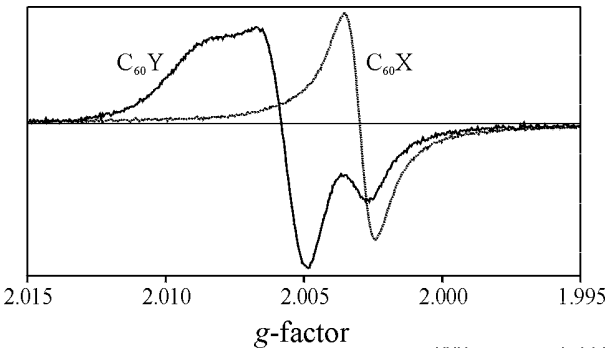

Fig. 3. ESR spectra of $C_{60}Y$ and $C_{60}X$ having the respective g-factors of 2.0058 and 2.0031.

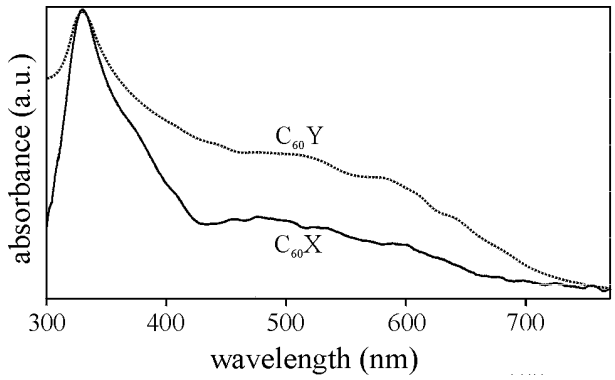

Fig. 4. Diffuse reflectance spectra of $C_{60}Y$ and $C_{60}X$, obtained by using NaY and NaX as the respective reference samples.

be inserted satisfactorily into the supercage of the faujasite zeolites in a vacuum without affecting the crystalline structure. Taking into account that C_{60} is a spherical molecule with a diameter of 0.70 nm, we have chosen faujasite zeolites as the matrices to take advantage of their three-dimensional supercage nanopores. The supercages are nanocavities having the diameter of 1.3 nm and they are tetrahedrally connected through 0.74 nm channels. The chemical shift of adsorbed xenon is reported to increase only if organic molecules are adsorbed inside zeolitic pores [33]. Our additional chemical shifts of 10 ppm for $C_{60}X$ and 6 ppm for $C_{60}Y$ with introducing 0.025 mol of C_{60} per molar supercage indicate that C_{60} molecules are really intercalated into the zeolitic nanocavities.

3.2 Formation of C_{60}^- in zeolitic nanocavities

As a neutral C_{60} molecule has no unpaired electron and does not give any ESR signal, the ESR spectra of Figure 3 indicate that the C_{60} adsorbed at the wall surface of the supercage gives birth to C_{60}^-. The produced radical species is stable enough to exist at the ground state. While bare NaX and NaY yield negligible ESR signals, $C_{60}X$ and $C_{60}Y$ bring in new intense sharp spectra with typical organic-radical g-values of 2.0031 and 2.0058, respectively. However, the g-values are significantly larger than those ($\sim$1.999) in solutions [10]. The large g-values are considered to arise from the polar environment of the radical anion in the supercage of the zeolites. The ESR spectrum of $C_{60}Y$ is much stronger and more anisotropic than that of $C_{60}X$. The stronger signal dictates that the radical anion forms more readily in NaY than in NaX. This is also supported by diffuse reflectance, time-resolved fluorescence, and transient reflectance (*vide infra*). The ESR spectrum of $C_{60}Y$ is too anisotropic to originate from a single species of C_{60}^- having the same surroundings. It seems to be superimposed with signals of polarized organic radicals split into multiplets by neighboring nuclear spins. On the other hand, the spectrum of $C_{60}X$ is isotropic and has a peak-to-peak linewidth ($\Delta H_{\rm pp}$) of 2 G. The $\Delta H_{\rm pp}$ of C_{60}^- is reported to be 60 G in solutions [10]. Hence, it is suggested that the collision-free environment of C_{60} isolated in zeolitic nanocavities results in the narrow linewidth. Nonetheless, Figure 3 clearly dictates that the radical anions of C_{60}^- exist at the ground state in the supercages of NaX and NaY.

3.3 Enhanced absorption of $t_{1u} \leftarrow h_u$ in zeolites

The diffuse reflectance spectra of Figure 4 reveal that C_{60} in faujasite zeolites has significantly strong broad absorption bands in the range of 410–620 nm together with the strong band at 330 nm. The strong peak at 330 nm, which is similar to the characteristic absorption of C_{60} in solutions [19], is assigned to the orbitally allowed transition of $t_{1g} \leftarrow h_u$. The broad absorption between 410 and 620 nm is attributed to the orbitally forbidden transitions of ${}^1t_{1u} \leftarrow {}^1h_u$ from C_{60} and ${}^2t_{1u} \leftarrow {}^2h_u$ from C_{60}^- [19]. These forbidden bands can appear weakly even in solutions because of local symmetry reduction resulting from solute-solvent interactions. Enhanced absorption in the visible band has also been observed as a result of charge-transfer interaction between fullerenes and electron donors such as polymeric films [27,28]. Accordingly, upon intercalation into the supercage of the zeolites the symmetry of C_{60} is distorted because the molecule interacts with the zeolitic surface. Hence, the absorption of C_{60} is predicted to enhance in the visible region. However, the absorption increase in the visible region is more likely contributed by the ${}^2t_{1u} \leftarrow {}^2h_u$ transition of C_{60}^- because it would possess even lower symmetry than C_{60}. Therefore, the significant absorption in the visible region supports the successful insertion of C_{60} and the anionic transformation of C_{60} in the supercages of NaX and NaY. The significantly strong visible absorption of Figure 4 also supports the ESR results that C_{60}^- is considerably more abundant in NaY than in NaX.

3.4 Dual and anionic fluorescence kinetics

The background-free fluorescence of C_{60} in the zeolites decays faster in the blue region than in the red region (Fig. 5). As shown with the fluorescence kinetic time constants (Tab. 1), our current experimental method can

Table 1. Background-free fluorescence kinetic constants of $C_{60}X$ and $C_{60}Y$, deconvoluted from Figure 5.

sample	emission wavelength (nm)	window time (ps)	fluorescence time constant (ps)	
			rise	decay
$C_{60}X$	435 ± 30	200	instant	28
	660+	200	instant (41%)[a] + 28	170 (41%) + 1 700
	660+	2 000	instant (51%) + 28	170 (51%) + 1 700
$C_{60}Y$	435 ± 30	200	instant	28
	660+	200	instant (52%) + 28	170 (52%) + 1 700
	660+	2 000	instant (74%) + 28	170 (74%) + 1 700

[a] Intensity percentage of each component at zero time delay.

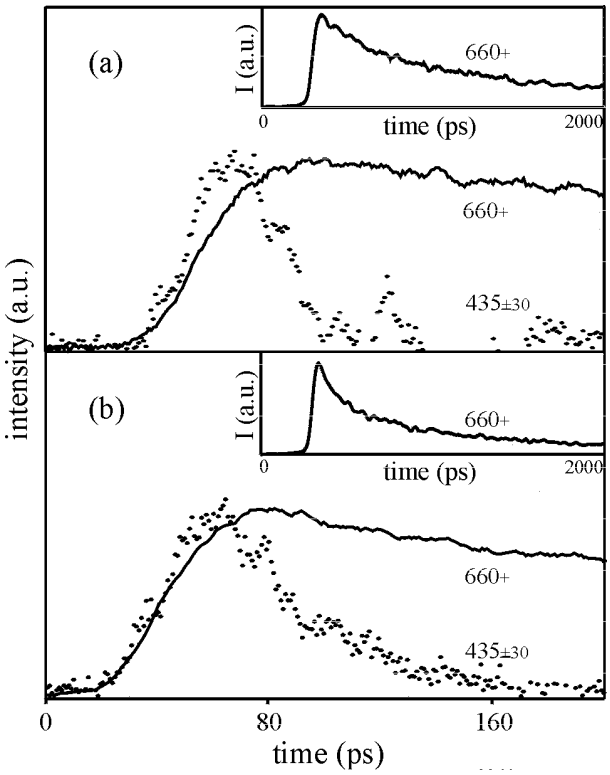

Fig. 5. Background-free fluorescence kinetic profiles, excited at 355 nm and monitored at shown wavelengths in nm, of $C_{60}X$ (a) and $C_{60}Y$ (b).

distinguish three fluorescence components that behave differently in time regime. The blue fluorescence decays in 28 ps to bring in the red fluorescence that decays on the time scale of 1 700 ps. Beside the slow decaying component, there is another red component that decays on the time scale of 170 ps. The blue component is ascribed to anomalous fluorescence emitted from the upper-excited $^1t_{1g}$ configuration of the neutral C_{60} species. The red component arising in 28 ps and decaying in 1 700 ps is assigned to the normal fluorescence emitted from the lowest excited $^1t_{1u}$ configuration of C_{60}. On the other hand, the red component appearing instantly and decaying in 170 ps is attributed to the anionic fluorescence emitted from the $^2t_{1u}$ configuration of C_{60}^-. Because of the anionic fluorescence rising instantly, the rise of the red fluorescence looks superficially faster than the decay of the blue fluorescence.

The kinetic constants in Table 1 show that the initial intensity percentage of the anionic fluorescence having the lifetime of 170 ps is greater in $C_{60}Y$ than in $C_{60}X$. This also confirms in the qualitative view that the anionic species can be formed more easily in NaY than in NaX. However, considering ESR signal and static absorption, we estimate that only a small fraction of C_{60} molecules transform into anions. The transition between the t_{1u} and h_u configurations is forbidden mainly because the fullerene has a center of inversion. As C_{60} adsorbs to the zeolitic surface, the selection rule becomes less strict. However, this becomes more significant for C_{60}^- because the anionic species interacts strongly with cations located at the surface. Even in solutions, forbidden transition is reported to be stronger for C_{60}^- than for C_{60} [29]. Therefore, adsorption to the surface of the zeolitic nanocavity exceedingly enhances the oscillator strength of the $^2t_{1u}$ emission of C_{60}^- in particular. Thus, although C_{60}^- is more abundant in $C_{60}Y$ than in $C_{60}X$, it is much scantier than C_{60} in both zeolites. Many research groups have reported on the fluorescence of C_{60} in solutions [20] or in solid films [25,28]. The static luminescence spectra of C_{60}-introduced zeolites [13–16] are shifted to the blue very significantly compared with those of C_{60}-dissolved solutions [20]. The upper-excited fluorescence of C_{60} certainly contributes to the spectral difference although the background luminescence present in C_{60}-free zeolites also does. It was recently reported that the normal and the anionic fluorescence spectra without the background luminescence have the intensity maxima at 750 and 770 nm, respectively, while the upper-excited fluorescence has the maximum at 450 nm in both NaY and VPI-5 [34,35].

3.5 Absorption spectra and dynamics of triplet and quartet states

While the time-resolved reflectance spectra of $C_{60}X$ show a strong absorption band with the maximum at 740 nm, those of $C_{60}Y$ show two comparable bands at 460 and 700 nm at the time delay of 15 μs (Fig. 6). The band of $C_{60}X$ at 740 nm is mostly due to the lowest triplet state

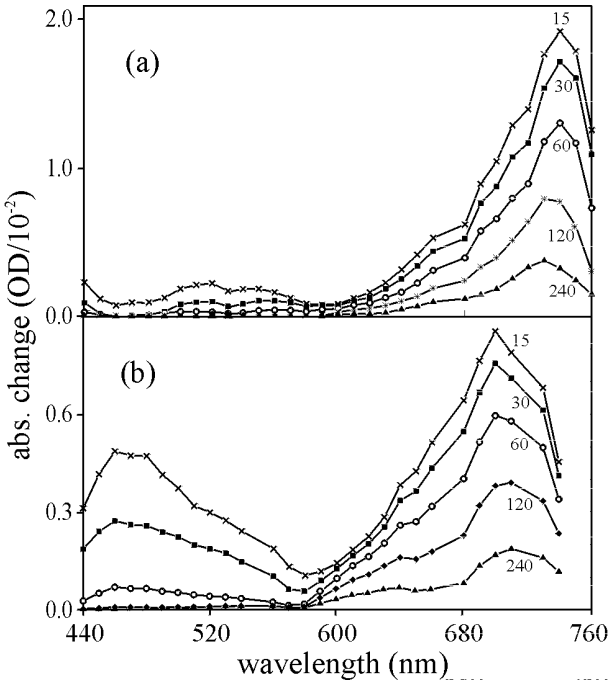

Fig. 6. Transient reflectance spectra, at the shown microsecond time delays after excitation at 337 nm, of $C_{60}X$ (a) and $C_{60}Y$ (b).

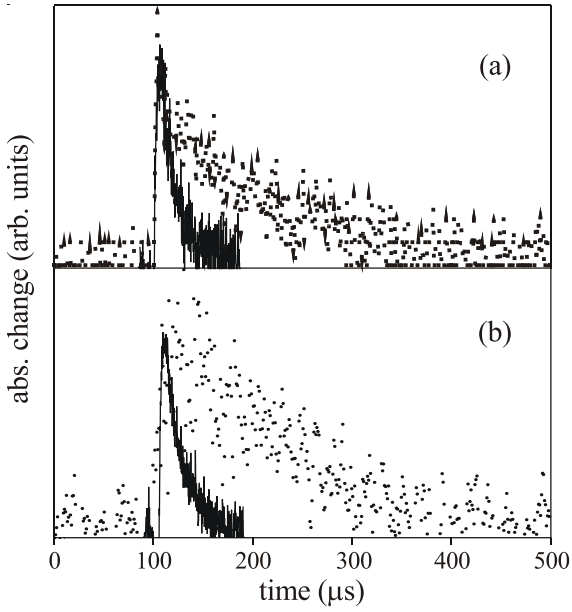

Fig. 7. Transient reflectance kinetic profiles, excited at 337 nm and probed at 490 (solid) and 720 nm (dotted), of $C_{60}X$ (a) and $C_{60}Y$ (b). The solid and dotted curves of both samples were fitted approximately to single exponential decays having the lifetimes of 25 and 140 μs, respectively, although the solid curve of $C_{60}X$ was found to have an additional slow component.

absorption ($T_n \leftarrow T_1$) of the neutral C_{60} species [27,28]. On the other side, the absorption band of $C_{60}Y$ at 460 nm results from the lowest quartet state absorption ($Q_n \leftarrow Q_1$) of the anionic C_{60}^- species [27,28]. Because of more anionic contribution, the red absorption band of $C_{60}Y$ at early time delays is shifted to the blue by 40 nm from the triplet state absorption band of $C_{60}X$. Both the weak band of $C_{60}X$ at 520 nm and the anionic band of C_{60} at 460 nm decay on a similar time scale. Thus it results mainly from the Q_1 absorption of C_{60}^-, which is reported to occur in the range of 350–520 nm. Then, Figure 6 also clearly shows that C_{60}^- is much more abundant in $C_{60}Y$ than in $C_{60}X$. The Q_1 state of C_{60}^- decays faster than the T_1 state of C_{60}. Figure 7 shows that in both zeolites the Q_1 state decays as fast as $(25\ \mu s)^{-1}$ while the T_1 state decays as slowly as $(140\ \mu s)^{-1}$. The T_1 state is known to relax on the time scale of 10–50 μs in solutions [25]. Our lifetime of 140 μs suggests that the quenching processes of the T_1 state such as T–T annihilation are greatly reduced for the C_{60} molecules isolated in zeolitic nanocavities as found in polymeric films [28]. The independent temporal behaviors of the two reflectance transients exclude the possibility that the T_1 state transforms into the Q_1 state following charge acceptance. The fast depopulation of the Q_1 state, compared with that of the T_1 state, is due to the stronger interaction of C_{60}^- with cations located at the zeolitic surface of the supercages. The strong interaction brings about a high spin-orbit coupling rate, leading to the fast relaxation of the Q_1 state into the ground state.

4 Discussion

Figure 1 schematically summarizes the equilibrium and photophysical dynamics of C_{60} and C_{60}^- intercalated in the supercages of NaX and NaY. The C_{60} molecules trapped in the supercages of NaX or NaY behave extremely differently from those in solvents or in the gas phase. Some of them transform into radical anions. The intensive electric field within the supercages of NaX and NaY [36], together with delocalized π electrons in C_{60} molecules, polarizes C_{60} molecules strongly enough to convert into C_{60}^- ions. The large g-values of the ESR spectra already have been ascribed to the ionic surroundings of C_{60}^- in the cavities. The relaxation of C_{60} or C_{60}^- excitation energy is slowed in the nanocavity. The relaxation of the upper-excited states in condensed phases is reported to take place within a few picoseconds [26]. However, the internal conversion from the upper-excited configuration of $^1t_{1g}$ to the first-excited configuration of $^1t_{1u}$ takes as long as 28 ps in the faujasite zeolites. The normal fluorescence lifetime of 1 700 ps and the lowest triplet state lifetime of 140 μs are much longer than the respective lifetimes in other circumstances [23,28]. We attribute the lifetime elongations mainly to the collision-free environment of C_{60} in the cavity. No report on the lifetimes of the lowest-excited doublet or quartet states probably comes from the fast relaxation of the anionic species. Thus the possible observation of 170 ps for the anionic fluorescence lifetime and 25 μs for the lowest quartet state lifetime also results from the relaxation-slow effect of the nanocavity. Nonetheless, the relaxation times of the lowest-excited doublet (170 ps)

and quartet states (25 μs) of the anionic species are much shorter than the respective values of the lowest-excited singlet (1 700 ps) and triplet states (140 μs) of the neutral species. We suggest that the interaction of two electrons above the h_u facilitates the relaxation of C_{60}^- excitation energy.

Placing an electron in the LUMO of t_{1u} to generate C_{60}^- reduces the symmetry, splitting the t_{1u} into a_{2u} and e_{1u} [37]. This symmetry reduction of C_{60}^- greatly increases the oscillator strength values of the visible absorption and the fluorescence that result from transition between t_{1u} and h_u configurations. This again dictates that the transformation efficiency of C_{60} into C_{60}^- is quite small although all the data from ESR, diffuse reflectance, and time-resolved fluorescence, and transient reflectance indicate the presence of C_{60}^-. Adsorption at the polar surface and strong interactions with cations enhance the oscillator strength of the symmetry-forbidden $t_{1u} \leftrightarrow h_u$ transition further.

It is quite intriguing that C_{60}^- is much more abundant in NaY than in NaX although the overall basicity of NaY is well-known to be weaker than that of NaX [38]. The dry supercages of both NaX and NaY are recently reported to be superpolar, even more polar than water [36]. We consider that this superpolarity of the zeolitic nanocavities leads C_{60} molecules to transform into C_{60}^- ions. It is also shown that the supercage of NaY is more polar than that of NaX and that an organic molecule trapped in the supercage of NaY experiences a stronger electric field than that in the supercage of NaX [36]. This explains qualitatively why more fractions of C_{60} molecules undergo reduction to form C_{60}^- in the supercages of NaY than in the supercages of NaX.

Thanks to the broad absorption ranging from the UV to the near IR, excited states of C_{60} and C_{60}^- can be optically generated easily from the ground states in the faujasite zeolites. We have shown above that encapsulation in zeolitic nanocavities suppresses the self-quenching processes of the lowest-excited singlet, doublet, triplet, and quartet states. The elongation of excited-state lifetimes is reported to increase the photocatalytic effect of the excited species [39,40]. The faujasite zeolites indeed change various characteristics of the inert species of C_{60} significantly.

5 Conclusions

C_{60} molecules have been intercalated into the supercages of NaX and NaY without affecting the crystalline structure at ∼650 °C. The superpolarity of zeolitic nanocavities facilitates C_{60} molecules to transform into C_{60}^- ions and even the higher superpolarity in NaY produces more C_{60}^- than in NaX. C_{60}-introduced zeolites have significantly strong visible absorption resulting from the allowed transition of C_{60}^- and the enhanced forbidden transition of C_{60} in the cavities. C_{60} in faujasite zeolites shows the dual fluorescence of the upper- and lowest-excited states having lifetimes of 28 and 1 700 ps, respectively. On the other hand, C_{60}^- shows monophasic fluorescence having a lifetime of 170 ps. The lowest triplet state of C_{60} has a lifetime of 140 μs with the absorption maximum at 740 nm while the lowest quartet state of C_{60}^- has a lifetime of 25 μs with the absorption maximum at 460 nm. We attribute the slow relaxation rates of C_{60} and C_{60}^- mainly to the collision-free environment of the zeolitic nanocavities. Strong interaction with the zeolitic surface and enhanced oscillator strength owing to reduced symmetry make C_{60}^- relax much faster than C_{60}.

The Center for Molecular Catalysis supported this work. D.J.J. and O.H.K. also acknowledge the Korea Research Foundation (KRF-2000-015-DP0193) and the Brain Korea 21 Program, respectively.

References

1. W. Chen, Z.G. Wang, Z.J. Lin, L.Y. Lin, Solid State Commun. **101**, 371 (1997).
2. K. Gaare, D. Akporiaye, J. Phys. Chem. B **101**, 48 (1997).
3. S. Takatani, H. Fukumura, H. Masuhara, S. Hashimoto, J. Phys. Chem. B **101**, 3365 (1997).
4. R. Ryoo, S.J. Cho, C. Pak, J.Y. Lee, Catal. Lett. **20**, 107 (1993).
5. N.R.B. Coleman, M.A. Morris, T.R. Spalding, J.D. Holmes, J. Am. Chem. Soc. **123**, 187 (2001).
6. Y.-J. Han, J.M. Kim, G.D. Stucky, Chem. Mater. **12**, 2068 (2000).
7. G.D. Stucky, J.E. Mac Dougall, Science **247**, 669 (1990).
8. H.W. Kroto, J.R. Heath, S.C. O'Brien, R.F. Curl, R.E. Smalley, Nature **318**, 162 (1985).
9. W. Krätschmer, L.D. Lamb, K. Fostiropoulos, D.R. Huffman, Nature **347**, 354 (1990).
10. C.A. Reed, R.D. Bolskar, Chem. Rev. **100**, 1075 (2000).
11. B. Hamilton, J.S. Rimmer, M. Anderson, D. Leigh, Adv. Mater. **5**, 583 (1993).
12. P.N. Keizer, J.R. Morton, K.F. Preston, A.K. Sugden, J. Phys. Chem. **95**, 7117 (1991).
13. G. Gu, W. Ding, G. Cheng, W. Zang, H. Zen, Y. Du, Appl. Phys. Lett. **67**, 326 (1995).
14. G. Gu, W. Ding, G. Cheng, S. Zhang, Y. Du, S. Yang, Chem. Phys. Lett. **270**, 135 (1997).
15. G. Sastre, M.L. Cano, A. Corma, H. García, S. Nicolopoulos, J. M. González-Calbet, M. Vallet-Regí, J. Phys. Chem. B **101**, 10184 (1997).
16. G. Gu, W. Ding, Y. Du, H. Huang, S. Yang, Appl. Phys. Lett. **70**, 2619 (1997).
17. T. Ito, J. Fraissard, J. Chem. Phys. **76**, 5225 (1982).
18. B.F. Chmelka, J.G. Pearson, S.B. Liu, R. Ryoo, L.C. de Menorval, A. Pines, J. Phys. Chem. **95**, 303 (1991).
19. S. Leach, M. Vervloet, A. Desprès, E. Bréheret, J.P. Hare, T.J. Dennis, H.W. Kroto, R. Taylor, D.R.M. Walton, Chem. Phys. **160**, 451 (1992).
20. B. Ma, Y.-P. Sun, J. Chem. Soc., Perkin Trans. **2**, 2157 (1996).
21. H.J. Byrne, W. Maser, W.W. Rühle, A. Mittelbach, W. Hönle, H.G. von Schnering, B. Movaghar, S. Roth, Chem. Phys. Lett. **204**, 461 (1993).

22. C. Reber, L. Yee, J. McKiernan, J.I. Zink, R.S. Williams, W.M. Tong, D.A.A. Ohlberg, R.L. Whetten, F. Diederich, J. Phys. Chem. **95**, 2127 (1991).
23. R.J. Sension, C.M. Phillips, A.Z. Szarka, W.J. Romanow, A.R. McGhie, J.P. McCauley Jr, A.B. Smith III, R.M. Hochstrasser, J. Phys. Chem. **95**, 6075 (1991).
24. T.W. Ebbesen, K. Tanigaki, S. Kuroshima, Chem. Phys. Lett. **181**, 501 (1991).
25. G. Sauvé, N.M. Dimitrijevic, P.V. Kamat, J. Phys. Chem. **99**, 1199 (1995).
26. R. Jacquemin, S. Kraus, W. Eberhardt, Solid State Commun. **105**, 449 (1998).
27. N.M. Dimitrijevic, P.V. Kamat, J. Phys. Chem. **97**, 7623 (1993).
28. M. Gevaert, P.V. Kamat, J. Phys. Chem. **96**, 9883 (1992).
29. M.A. Greaney, S.M. Gorun, J. Phys. Chem. **95**, 7142 (1991).
30. M.M. Alam, M. Sato, A. Watanabe, T. Akasaka, O. Ito, J. Phys. Chem. A **102**, 7447 (1998).
31. T. Kato, T. Kodama, T. Shida, Chem. Phys. Lett. **205**, 405 (1993).
32. L.C. de Menorval, D. Raftery, S.-B. Liu, K. Takegoshi, R. Ryoo, A. Pines, J. Phys. Chem. **94**, 27 (1990).
33. R. Ryoo, S.-B. Liu, L.C. de Menorval, K. Takegoshi, B. Chmelka, M. Trecoske, A. Pines, J. Phys. Chem. **91**, 6575 (1987).
34. O.-H. Kwon, H. Yoo, K. Park, B. Tu, R. Ryoo, D.-J. Jang, J. Phys. Chem. B **105**, 4195 (2001).
35. O.-H. Kwon, K. Park, D.-J. Jang, Chem. Phys. Lett. **346**, 195 (2001).
36. S. Uppili, K.J. Thomas, E.M. Crompton, V. Ramamurthy, Langmuir **16**, 265 (2000).
37. D.R. Lawson, D.L. Feldheim, C.A. Foss, P.K. Dorhout, C.M. Elliott, C.R. Martin, J. Electrochem. Soc. **139**, L68 (1992).
38. X. Liu, K.-K. Iu, J.K. Thomas, J. Phys. Chem. **98**, 7877 (1994).
39. M. Brink, H. Jonson, M. Sundahl, J. Photochem. Photobiol. A: Chem. **112**, 149 (1998).
40. H. Möllerstedt, O. Wennerström, J. Photochem. Photobiol. A: Chem. **139**, 37 (2001).